

Quantifying the benefits of a slender, high tip speed blade for large offshore wind turbines

Lindert Blonk, Patrick Rainey, David AJ Langston and Francesco Vanni

DNV GL, Silverthorne Lane, Bristol, BS2 0QD, UK

lindert.blonk@dnvgl.com

Abstract. An in-depth study has been completed to study the effects of slender, flexible blades in combination with high rotor speed operation on load mitigation, targeted at cost reductions of the structural components of large wind turbines, consequently lowering the levelized cost of energy. An overview of existing theory of sensitivity of turbine fatigue loading to the blade chord and rotor speed was created, and this was supplemented by a proposed theory for above-rated operation including the pitch controller. A baseline jacket-supported offshore turbine (7MW) was defined, of which the blade was then redesigned to be more slender and flexible, at the same time increasing rotor speed. The blade redesign and optimisation process was guided by cost of energy assessments using a reduced loadset. Thereafter, a full loadset conform IEC61400-3 was calculated for both turbines. The expected support structure load reductions were affirmed, and it was shown that reductions of up to 18.5 % are possible for critical load components. Cost modelling indicated that turbine and support structure CapEx could be reduced by 6%. Despite an energy production reduction of 0.44% related to the thicker airfoils used, the blade redesign led to a reduction in Cost of Energy.

1. Introduction

A key challenge to improve the economics of offshore wind energy – and thereby sustained public and political support for large programs – is lowering the cost of the structural components of large wind turbines and their support structures. The hypothesis is that increasing design rotor speeds in combination with significant reductions to blade chord lengths and blade stiffness can mitigate loading on these components, hence reducing their cost and wind farm cost of energy. The authors have completed an in-depth assessment to these effects, the results of which are presented here.

The study was conducted throughout 2013 in the context of the DNV GL Garrad Hassan FORCE project (*FOR* Reduced Cost of Energy), a research project aimed at fully integrated design of large offshore wind turbines. This *FORCE* project consisted of two phases: phase I, where the use of advanced control strategies was demonstrated, and phase II, which focused on the blade redesign and is discussed in this paper. This research aims to compliment other studies in the field of integrated turbine design [3][4].

The research discussed in this paper uses two approaches. The first approach, described in section 2, is a theoretical approach; an investigation to the scaling relations that describe the dependence of turbine fatigue loading to changes in design rotor speed and blade chord lengths. The second approach, described in section 3, is a full design study comparing a high speed, slender rotor turbine to a baseline turbine, using aero-hydro-elastic time history based load calculations and assessment of cost effects using cost models.



2. Theoretical approach

Theory is proposed here that aims to predict how fatigue loading varies when the turbine design rotor speed is changed and the rotor chords are re-optimized for the new rotor speed. The theory focuses solely on aerodynamically induced loading; inertial effects are not included. The summary results of the analysis are presented in Table 1, with the derivation given in the following sub-sections. The expected load scaling depends on whether the turbine is operating above or below rated wind speed and is also different for high and low frequency wind speed variation. The low frequency response relates to the gradually changing steady state thrust as the wind speed changes, while the high frequency response relates to fast changes in wind speed where the pitch system response does not dominate. In summary, fatigue loading is expected to reduce for increased design tips speed ratios (λ).

Table 1: expected scaling of fatigue loading with rotor design parameters

wind speed regime	section	wind speed perturbation frequency range	thrust variance scaling with design tip speed ratio
below rated	2.1.1.	low frequency	λ^0
below rated	1.1.	medium to high	λ^{-1}
above rated	2.2.1.	low frequency	λ^0
above rated	2.2.5.	high frequency	between λ^{-1} and λ^{-3}

2.1. Scaling relations in the constant pitch region (below rated wind speed)

2.1.1. Low frequency thrust variation

For low frequency wind perturbations we expect the thrust to be governed by the basic relationship $Power = Thrust \times Wind\ speed$, which is independent of rotor speed and chord, i.e. scales as $\Omega_{rated}^0, c^0, \lambda^0$.

2.1.2. High frequency thrust variation

A load change as a result of wind speed perturbation for the case of constant pitch position is described in the Wind Energy handbook [1], and copied into (1). Here ΔL is the change in lift force, Δu is the variation of wind speed incident on the airfoil, α is the angle of attack, ρ is the air density, c is the blade chord, r is the radial position along the blade, Ω is the rotor speed, and C_L is the lift coefficient.

$$\Delta L = \Delta u \frac{dL}{du} = \frac{1}{2} \rho (\Omega r)^2 c \frac{dC_L}{d\alpha} \frac{\Delta u}{\Omega r} = \frac{1}{2} \rho \Omega r c \frac{dC_L}{d\alpha} \Delta u \quad (1)$$

$$\Delta L \sim \Omega c \sim \lambda c \quad (2)$$

Here, we consider the case where rated rotor speed scales approximately with design tip speed ratio. Optimal chord scales with the inverse of the design tip speed ratio squared [2]:

$$c(\lambda, r) = \frac{16\pi R^2}{9BC_{L,d}\lambda^2 r} \quad (3)$$

where B is the number of blades, $C_{L,d}$ the design lift coefficient. Thus,

$$c \sim \lambda^{-2} \quad (4)$$

Although it is likely that chords in a physical blade design will deviate significantly from the optimal chordline, this line can be taken as indicative for the relative changes in chord when increasing design rotor speed. Substituting eq (4) in (2) yields (5).

$$\Delta L \sim \lambda^{-1} \quad (5)$$

2.2. Scaling relations in the variable pitch region (above rated wind speed)

2.2.1. Low frequency thrust variation

For low frequency wind perturbations we still expect the thrust to be governed by the basic relationship $Power = Thrust \times Wind\ speed$, just as below rated wind speed. The difference here is that above rated the power is constant so the thrust decreases with increasing wind speed. It is still independent of rotor speed and chord, so again scales as $\Omega_{rated}^0, c^0, \lambda^0$.

2.2.2. Derivation of transfer functions

To derive scaling laws above rated the closed loop system including the pitch-speed controller must be considered in the analysis. For this purpose a two input – two output linear model of the rotor was considered, expressed here as a matrix equation of transfer functions. The transfer functions are written as functions of s to indicate that all equations are in the Laplace domain. Each of the elements of the transfer function matrix are named G followed by two subscripts. The two subscripts reference the inputs and outputs that that transfer function relates to, e.g. $G_{TU}(s)$ is the transfer function from wind speed to thrust while $G_{\Omega\beta}(s)$ is the transfer function from pitch angle to rotor speed. The only assumptions are that the wind speed can be considered as a single input rather than a field over the rotor and that the turbine can be considered as a linear system.

$$\begin{bmatrix} \Delta Thrust \\ \Delta Rotor\ speed \end{bmatrix} = \begin{bmatrix} G_{TU}(s) & G_{T\beta}(s) \\ G_{\Omega U}(s) & G_{\Omega\beta}(s) \end{bmatrix} \begin{bmatrix} \Delta Wind\ speed \\ \Delta Pitch\ angle \end{bmatrix} \quad (6)$$

Of the two inputs to this model, the wind speed can be viewed as the disturbance whose effect we wish to minimise, while the pitch angle is an internal variable that responds to the wind disturbance through the rotor speed response and the controller. We can express both the thrust and the rotor speed as dependant on the wind speed alone once we consider the controller, $C(s)$, which is a transfer function from rotor speed to pitch angle:

$$\beta(s) = C(s) * \Delta Rotor\ speed(s) \quad (7)$$

Substituting (7) into the bottom row of (6):

$$\Delta Rotor\ speed(s) = G_{\Omega U}(s)\Delta U(s) + G_{\Omega\beta}(s)C(s) * \Delta Rotor\ speed(s) \quad (8)$$

And rearranged to give:

$$\Delta Rotor\ speed(s) = \frac{G_{\Omega U}(s)}{1 - C(s)G_{\Omega\beta}(s)} \Delta U(s) \quad (9)$$

Substituting (7) then (9) into the top row of (6):

$$\Delta Thrust(s) = G_{TU}(s)\Delta U(s) + G_{T\beta}(s)C(s) \frac{G_{\Omega U}(s)}{1 - C(s)G_{\Omega\beta}(s)} \Delta U(s) \quad (10)$$

$$= \left(G_{TU}(s) + \frac{G_{\Omega\beta}(s)C(s)G_{\Omega U}(s)}{1 - C(s)G_{\Omega\beta}(s)} \right) \Delta U(s) \quad (11)$$

The variation in thrust with wind speed has thus been broken down into various transfer functions relating to the rotor plus the controller. These transfer function will be quite complex in reality as they include all the dynamics of the system, few assumption have been made so far. Next simplifying assumptions must be made to create a simple theory of how each of these functions scale.

2.2.3. Scaling of the transfer functions

The key simplifying assumption that was used was to consider that the scaling of the transfer functions will follow the scaling of the lift force on the blade. It should be clear that the thrust on the structure is dominated by the lift on the blades. The rotor speed is determined by the rotor acceleration which is driven by difference between the aerodynamic driving force and the electrical resistance from the generator. The downside to this assumption is that drag is not considered and this might make a significant contribution to the aerodynamic driving force.

The lift variation with wind speed can be modelled as in (1), while the lift variation with pitch angle is equivalent to direct variation of angle of attack.

$$L = \frac{1}{2}\rho(U^2 + \Omega^2 r^2)cC_l(\alpha) \quad (12)$$

$$\frac{\partial L}{\partial U} \approx \frac{1}{2}\rho(U^2 + \Omega^2 r^2)c \frac{\partial C_l}{\partial \alpha} \frac{1}{\Omega r} \quad (13)$$

$$\frac{\partial L}{\partial \beta} = -\frac{1}{2}\rho(U^2 + \Omega^2 r^2)c \frac{\partial C_l}{\partial \alpha} \quad (14)$$

These equations can be used to establish scaling laws for the transfer functions in our linear model. Our assumption that the transfer functions are dominated by lift translates into assuming that G_{TU} and $G_{\Omega U}$ scale with $\frac{\partial L}{\partial U}$, while $G_{T\beta}$ and $G_{\Omega\beta}$ scale with $\frac{\partial L}{\partial \beta}$. As turbines usually operate with tip speed ratios much greater than one, we use $(U^2 + \Omega^2 r^2) \approx \Omega^2 r^2$ to give clean scaling with rotor speed. Table 2 lists the scaling relationships for each of the transfer function expressed in rotor speed and chord, treating each as independent, then also in terms of tip speed ratio using $c \propto \lambda^{-2}$ and $\Omega \propto \lambda^1$.

Table 2: Scaling laws for the transfer functions

Function	Scaling with rotor speed	Scaling with chord	Scaling with TSR
$G_{TU}(s)$	Ω^1	c^1	λ^{-1}
$G_{T\beta}(s)$	Ω^2	c^1	λ^0
$G_{\Omega U}(s)$	Ω^1	c^1	λ^{-1}
$G_{\Omega\beta}(s)$	Ω^2	c^1	λ^0

Using these scaling relationships we can separate out the rotor speed and chord dependant parts of the transfer functions. For example $G_{TU}(s) = K_{TU}(s)\Omega^1 c^1$, where $K_{TU}(s)$ should be independent of rotor speed setpoint and blade chord. Note that we refer to Ω as the rotor speed setpoint to distinguish it from $\Delta Rotor\ speed$. $G_{TU}(s)$ is assumed to be a constant function as the rotor speed varies around the setpoint even though it is clear in the underlying equations that the partial derivatives vary as the rotor speed varies around the setpoint.

2.2.4. Rotor Speed Variation and Equivalent Controllers

The scaling of the controller transfer function will depend on what control objectives are used to tune the controller. For this analysis, the primary controller objective was taken to be ‘to keep the rotor speed variation caused by turbulence to within a set proportion of the rated rotor speed’. Defining it like this we allow the rotor speed variation to scale as Ω^1 or λ^1 . Consider first the case of only changing the rated rotor speed. Taking (9) and substituting $G_{\Omega U}(s) = K_{\Omega U}(s)\Omega^1 c^1$ and $G_{\Omega \beta}(s) = K_{\Omega \beta}(s)\Omega^2 c^1$ we get:

$$\Delta \text{Rotor speed}(s) = \frac{K_{\Omega U}(s)\Omega^1 c^1}{1 - CK_{\Omega \beta}(s)\Omega^2 c^1} \Delta U(s) \quad (15)$$

In this case if the controller, C , scales as Ω^{-2} , then the denominator is invariant of rotor speed setpoint, and the rotor speed variations would scale with the speed setpoint as required. However if the chord also changes then the associated controller change is more complex:

$$\Delta \text{Rotor speed}(s) = \frac{K_{\Omega U}\lambda^{-1}}{1 - CK_{\Omega \beta}} \Delta U(s) \quad (16)$$

At high frequencies, $CK_{\omega \beta}$ is generally small and the variation of rotor speed fraction will decrease with increasing λ regardless of the controller. At lower frequencies, the controller can scale as λ^{-2} , or ω^{-2} , just as in the case of constant chord. We will continue to write the controller as scaling with λ^{-2} , but will bear in mind that it could reduce faster than this, especially at high frequencies.

2.2.5. High frequency thrust variation

In high frequencies both $C(s)$ and $G_{\Omega \beta}(s)$ tend to zero, the controller because of low pass roll off filters, and the system because of the rotor inertia. At sufficiently high frequencies $C(s)G_{\Omega \beta}(s) \ll 1$ so the transfer function for thrust from wind speed simplifies to:

$$\Delta \text{Thrust}(s) = (G_{TU}(s) + G_{T\beta}(s)C(s)G_{\omega U}(s))\Delta U(s) \quad (17)$$

which has the scaling:

$$\begin{aligned} \Delta \text{Thrust}(s) &= (K_{TU}(s)\omega^1 c^1 + K_{T\beta}(s)\omega^2 c^1 C_0(s)\omega^{-2} G(s)K(s)\omega_U \omega^1 c^1)\Delta U(s) \\ &= (K_{TU}(s)\omega^1 c^1 + K_{T\beta}(s)C_0 K_{\omega U}(s)\omega^1 c^2)\Delta U(s) \\ &= (K_{TU(s)}\lambda^{-1} + K_{T\beta(s)}C_0 K_{\omega U}(s)\lambda^{-3})\Delta U(s) \end{aligned} \quad (18)$$

The conclusion therefore is that if the tip speed ratio and rated rotor speed are increased with an accompanying reduction of chord and controller gain then the high frequency thrust variation will decrease partly inversely and partly as λ^{-3} , as stated in Table 1. Note however that the controller gains can scale faster than λ^{-2} , especially at high frequencies, so it may still be possible to reduce the thrust variation further, however at low frequencies the thrust variation will be invariant.

3. Full design study

The second approach to assessment of the potential of high speed slender rotors to reduce turbine cost was a full design approach comprised of blade redesign, followed by loads simulations and reoptimization of the turbine structural components. Each of these tasks takes significant engineering effort, so the theoretical foundations established in Section 2 were used to guide design choices. Reduction of blade chord has simple benefits in terms of load reduction for the idling case or when rotor speed effects are ignored. However, the theoretical analysis showed that load reductions can be expected, even when the chord reductions are accompanied by an increase in rotor speed.

A 3-bladed turbine design was selected as baseline, based on commercial experience, to be representative of the current state-of-art in large offshore turbines and for the UK round 3 windfarms. Its characteristics are described in Table 3 and the characteristics of the blade in Table 4.

Rated power	7MW
Rotor speed	10.74rpm
Gearbox ratio	37.714
Water depth	40m
Rotor diameter	160m
Nacelle mass	380t
Rotor mass	205t
Blade mass	35t
Tower mass	310t
Jacket and transition mass	900t
Piles (each of 4)	147t

Table 3: Baseline turbine properties



Figure 1: View of bladed model for the baseline turbine

The controller for the baseline turbine included a torque-speed control loop for below rated operation, a pitch-speed loop (inclusive of a nacelle acceleration feedback term for tower damping) for above rated operation, a drivetrain damping term and a 1P individual pitch control (IPC) loop above rated. It also included a 2P IPC control loop and a LiDAR-based (Light Detection and Ranging) feedforward control term.

The blade was redesigned using an in-house structural blade design tool. The tool is used for blade design in conceptual stages of turbine design and is based on section analysis according to Timoshenko beam theory for composite beams. The tool divides the blade sections into surface elements and the contributions of the individual elements are summed to find the section mass and stiffness properties. 40 sections per blade were analysed. The effect of mass changes in the outboard region of the blade to the gravity-induced blade root fatigue loading was accounted for in the blade structural redesign. Both the baseline and the updated blade used glass fiber spar caps. Compressive strains on the suction side of the blade were most critical in dimensioning the spar. The addition of 2P Individual Pitch Control and LiDAR to the turbine controller in earlier stages of the FORCE project had led to reduced flapwise fatigue load levels. This alleviation was utilized in the blade redesign and allowed further chord reductions. The chord lengths were reduced along the blade span by up to 20%. The tips speed ratio was increased from 9.0 to 10.0, and the maximum tip speed was increased from 90 m/s to 100 m/s. Maximum tips speed does not increase beyond 100 m/s as this could lead to excessive blade leading-edge erosion. To maintain sufficient tower clearance with the slender and more flexible blade, prebend was added. The high speed blades' chord and thickness distribution were optimised for cost of energy through several design iterations, using the Garrad Hassan turbine and wind farm cost models to trade-off energy yield against blade structural design and drivetrain design considerations. A summary of blade properties for the baseline and new blade is given in Table 4.

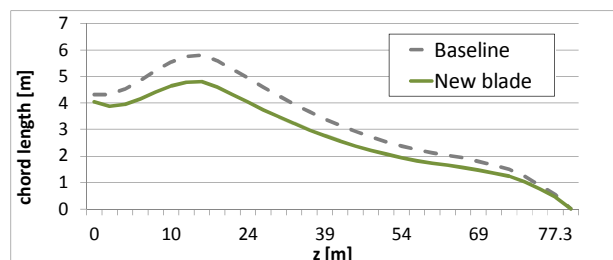


Figure 2: chord distributions

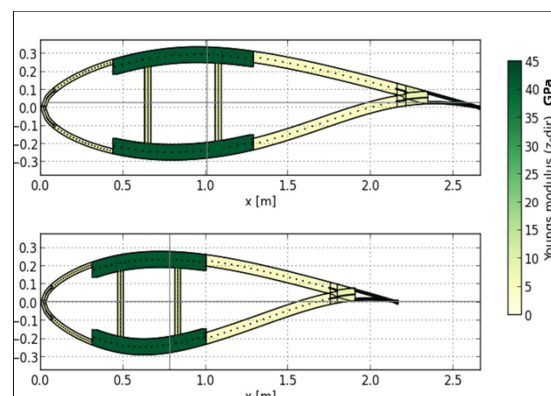


Figure 3: Output of structural concept blade design tool; blade cross-section at $z=50\text{m}$, baseline (top) and new blade (bottom)

Table 4: Blades properties

Δ from root	baseline data				Ratios: high-speed blade / baseline blade			
	chord	thickness/ chord	flapwise bending stiffness	mass per unit length	chord	thickness /chord	flapwise bending stiffness	mass per unit length
[m]	[m]	[%]	[GNm ²]	[kg/m]	[-]	[-]	[-]	[-]
0	4.3	100	100	2900	0.94	1	0.94	1
20	5.4	35	4.9	540	0.82	1.05	0.76	1.05
40	3.3	25	0.86	380	0.81	1.08	0.74	1.09
60	2.1	21	0.11	200	0.81	1.09	0.75	1.08

Dynamic load computations were performed using multi-body GH Bladed for the baseline and redesigned turbine, according to IEC61400-3, using IEC class 1A wind conditions, site specific directional wave loading based on data recorded at Dogger Bank, North Sea (30-40m depth), and a fully defined jacket support structure. A detailed turbine model was built in Bladed that included sufficient modal frequencies to capture the dynamics of the turbine across the load /operational envelope. Crucially, the flapwise, edgewise and torsional modes of the blade were modelled, so that the complex behaviour of the slender flexible blades could be captured. Further to this, the fore-aft, side-side and torsional modes of the support structure were also included to enable the coupled behaviour of the whole system to be modelled.

The resulting high resolution load case definition provided 456 fatigue load simulations which were done for both the baseline and the redesigned turbine, covering operational, fault and idling load cases. The extreme load calculations were of similar detail but focused on the load cases that result on high rotor and support structure loads. SACS software was used in the support structure analysis and optimisation.

To quantify the effect of the changed loading on the cost of energy a second turbine design iteration was carried out, with the newfound load levels as an input. The iterative process of *turbine redesign - load calculation - turbine redesign* ended at this stage; it was thus assumed that the loads would not change significantly following the reoptimization of the components. The support structure and tower were manually re-optimized for the new load levels. The blades' layup thicknesses (not the aerodynamic profile) were re-optimized using the above described conceptual blade design tool. The effects of the load changes on component mass for the remaining components were assessed using the GH component cost models, which are sensitive to load inputs. The CoE models have been developed over a number of years by Garrad Hassan (now DNV-GL) and the principles are summarized in

schematic form in Figure 4. The models of the turbine, the balance of plant characteristics and the operation and maintenance, are used to calculate the economic outputs of CAPEX, OPEX, which in turn are used to calculate the CoE. A Fixed Charge Ratio (FCR) of 12.5% has been used.

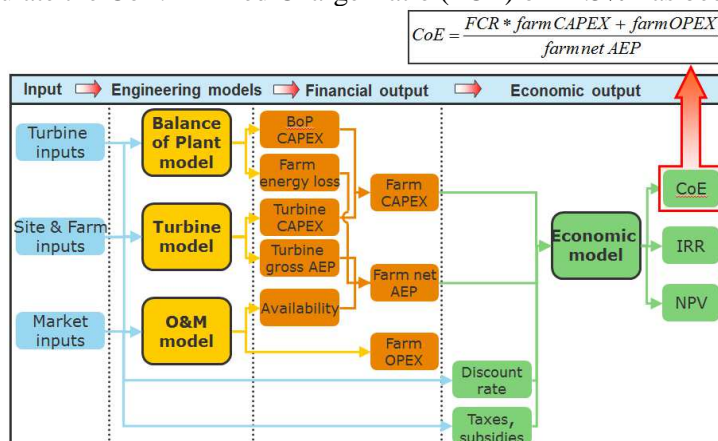


Figure 4: Cost model schematic diagram

4. Results

4.1. Results of load calculations

All loading and CoE results discussed below are expressed in terms of percentage changes from the baseline turbine and controller configuration. The baseline controller had to be re-tuned for the slender blade, but the same tuning criteria adopted for the baseline were followed, so the differences between the results can be attributed to the blade and rotor speed changes only. The blade flapwise extreme bending moment was reduced by 10%. Fatigue Damage Equivalent Loads (DEL's) were reduced significantly for most key load components on the turbine and support structure. The fatigue load changes at several interfaces are given in Table 5.

Table 5: Changes to Damage Equivalent Loads

Slope of the S/N curve	Load component	Load change	Slope of the S/N curve	Load component	Load change
S/N = 10	Blade 1 Mx [kNm]	8.0 %	S/N = 4	Stationary hub Mx [kNm]	-16.0 %
	Blade 1 My [kNm]	-9.4 %		Stationary hub My [kNm]	3.5 %
	Blade 1 Mz [kNm]	21.7 %		Stationary hub Mz [kNm]	-4.6 %
	Rotating hub Mx [kNm]	-16.0 %		Stationary hub Fx [kN]	-8.73 %
S/N = 4	Rotating hub My [kNm]	5.3 %	S/N = 4	Yaw bearing Mx [kNm]	-15.1%
	Rotating hub Mz [kNm]	5.6%		Yaw bearing My [kNm]	-2.4%
	Rotating hub Fx [kN]	-8.7%		Yaw bearing Mz [kNm]	-2.7%
				Yaw bearing Fx [kN]	-18.5%
				Annual Energy production	-0.44%

The blade My (flapwise) moment, which is critical in determining minimal blade thickness, was reduced significantly. Review of a selected number of loadcases showed that it is likely that the increase in the fatigue blade root Mz load is related to the impact on the flap-twist coupling of the reduction in blade-stiffness, however this requires further investigation to confirm. For the aerodynamic thrust related load components; blade root My and hub Fx, the total load reduction is of the order of 10%, which is within the bounds given by theoretical predictions. A notable load reduction is the reduction in the tower top thrust load (fatigue yaw bearing Fx). This load component

is the main driver for the jacket and tower design. The load reduction occurs both below and above rated wind speed as illustrated in Figure 5.

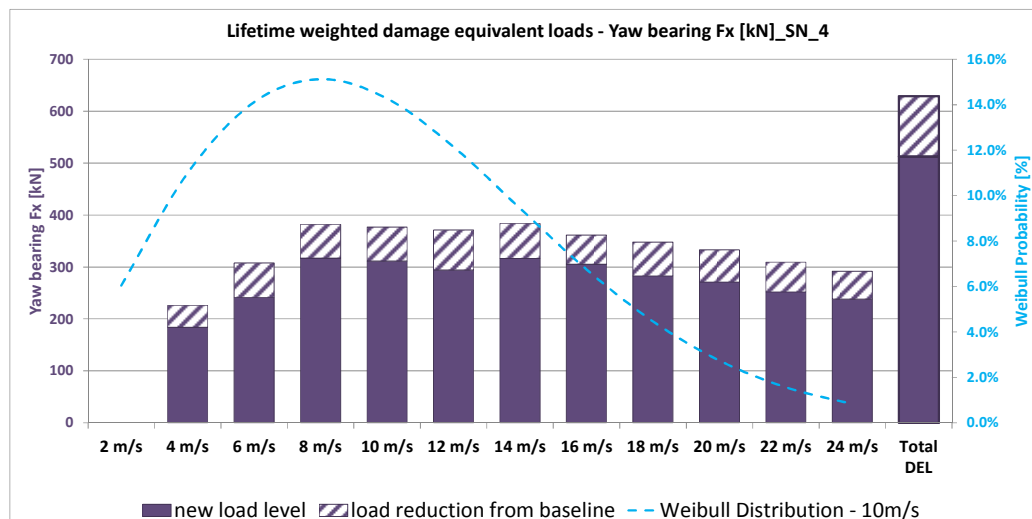


Figure 5: fatigue load changes for the jacket and tower design driving Fx (parallel to wind) load component at yaw bearing (tower top) level

Further investigations indicated that some of the Fx load alleviation is attained at low frequencies which is a deviation from the previously described theory (Table 1). Additionally, at low wind speeds, further alleviation is attained in the frequency range between the tower frequency and the 3P excitation frequency of the rotor, due to greater separation of these, as illustrated in Figure 6. Note that the cumulative variance is the integral of the power spectral density, where the power spectral density is calculated as described in [5]. The reduction in AEP is due to the increases in airfoil thicknesses.

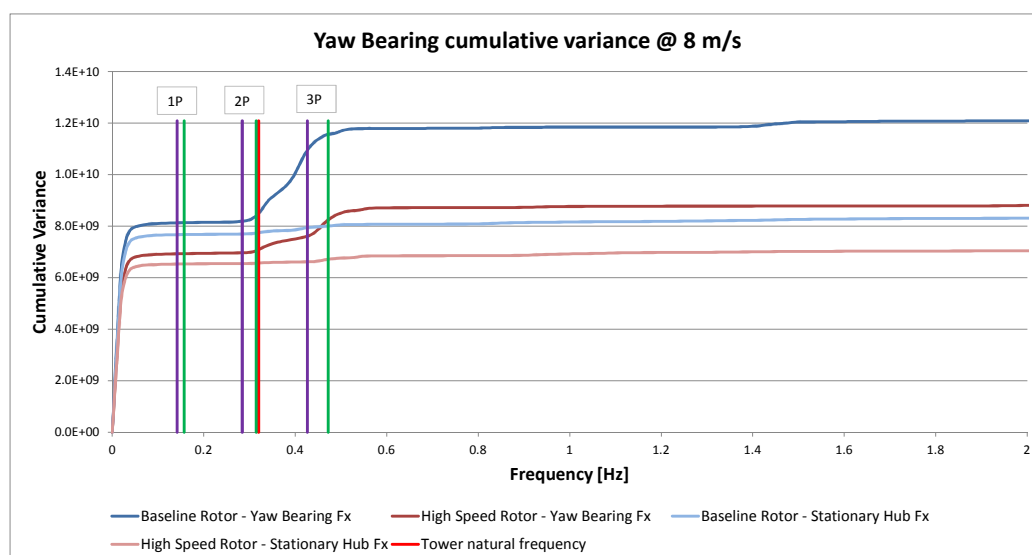


Figure 6: Cumulative variance for the hub Fx and yaw Fx load. The excitation frequencies of the baseline and high speed rotor are indicated by the purple and green vertical lines, respectively.

4.2. Result of analysis to cost effects

Since the flapwise moment load reductions were larger than anticipated during the initial slender blade design, the re-optimization the blade, part of the cost modelling analysis described at the end of

section 3, resulted in a slightly lighter-than-baseline blade and hence lower cost. The re-optimization of the jacket support structure yielded a 8% mass reduction due to the lower fatigue loading. Mass reductions were also achieved in the hub, main shaft, mainframe and tower. The drivetrain mass was reduced by 10% due to the lower rated torque. Overall, the CoE reduction related to the blade redesign was 2.2%, including the effect of the AEP reduction of 0.44%. The Capital Expenditure for the turbine, including the support structure, was reduced by 6%.

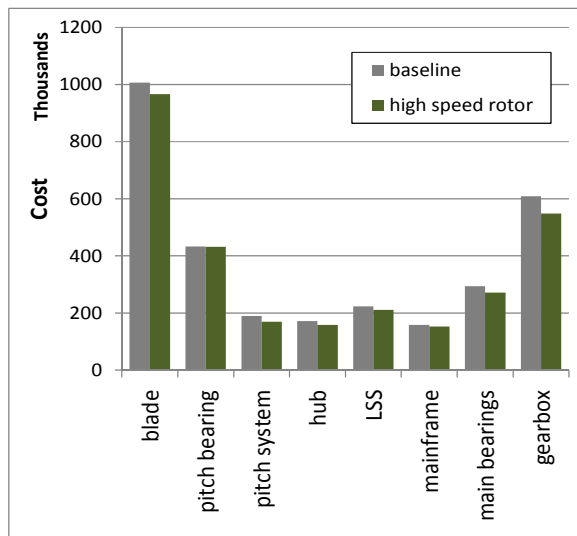


Figure 7: Cost changes for RNA (Rotor Nacelle Assembly) components

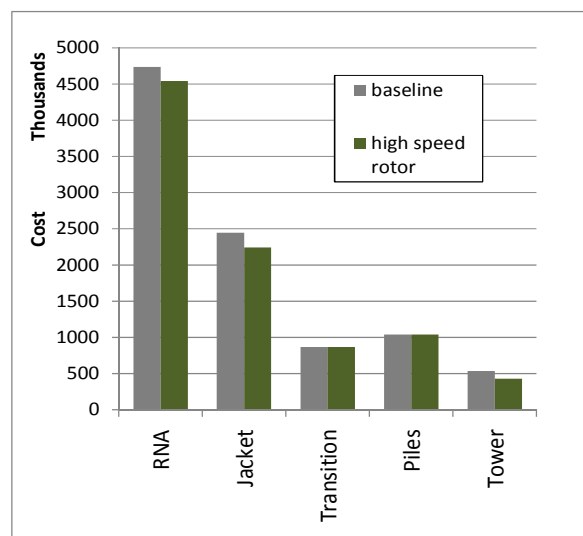


Figure 8: Main turbine component cost changes

5. Conclusion

Theories were reviewed and further developed which predicted fatigue load reductions due to lower aerodynamic excitation when increasing rotor speed whilst decreasing blade chord lengths. These theories included the effect of the pitch controller. A thorough design comparison study was conducted, to assess the potential of the fatigue reduction mechanisms identified through theory. A large (7MW) offshore baseline turbine was defined which included a jacket support structure. The blades were redesigned for higher speed operation (10% increase of speed). The evaluations of a full load calculation according to IEC61400-3 affirmed the lower fatigue loading levels for the slender, high-speed rotor. Reductions of the order of magnitude of 10% were found for a selection of design driving fatigue load components. A particularly favourable load reduction of 18.5% resulted for the damage equivalent tower top axial force; a load component that strongly influences the cost of the support structure. Structural redesign of the jacket support structure showed that its weight could be reduced by 8%. Cost modelling indicated that the Cost of Energy reduction is 2.2%, and the turbine and support structure CapEx reduction 6%.

References

- [1] T. Burton, D. Sharpe, N. Jenkins, E. Bossany, *Wind Energy Handbook*, 2001
- [2] P. Jamieson, *Innovation in wind turbine design*, 2011
- [3] T. Fischer, W. de Vries, P. Rainey, B. Schmidt, K. Argyriadis, M. Kühn, *Offshore support structure optimization by means of integrated design and controls*, Wind Energy, The UpWind Special Issue, Volume 15, Issue 1, January 2012
- [4] W. Xudong, W. Z. Shen, W. J. Zhu, J. N. Sørensen, C. Jin, *Shape optimization of wind turbine blades*, Wind Energy, Volume 12, Issue 8, November 2009
- [5] M. Cerna and A. F. Harvey, *The Fundamentals of FFT-Based Signal Analysis and Measurement*, National Instruments, Application note 41, 2000